First publ. in: Journal of Structural Biology 128 (1999), 2, pp. 187-199

Quantitative Energy-Dispersive X-Ray Microanalysis of Calcium Dynamics in Cell Suspensions during Stimulation on a Subsecond Time Scale: Preparative and Analytical Aspects as Exemplified with *Paramecium* Cells

Martin Hardt and Helmut Plattner[1]

Faculty of Biology, University of Konstanz, P.O. Box 5560, D-78434 Konstanz, Germany

Received June 25, 1999, and in revised form August 20, 1999

We analyzed preparative and analytical aspects of the dynamic localization of Ca^{2+} during cell stimulation, using a combination of quenched flow and energy-dispersive X-ray microanalysis (EDX). Calcium (or Sr, as a substitute) was retained as fluorides during freeze-substitution, followed by epoxide embedding. The quenched-flow used allowed analyses, during stimulation, in the subsecond time range. Sections of 500 nm were analyzed and no artificial Ca or Sr leakage was recognizable. We calculated a primary beam spread from 63 to 72 nm that roughly indicated the resolution of EDX/structure correlation. These values are quite compatible with the size of potential structures of interest, e.g., Ca stores (~100-nm thickness) or cilia (~250-nm diameter). We used widely different standards to calibrate the ratio of CaK_α net counts in relation to actual [Ca]. Calibration curves showed a linear relationship and a detection limit of [Ca] = 2 mM, while [Ca] in cytosol was 3 mM and in stores was 43 mM, both in nonactivated cells. Eventually Sr^{2+} can rapidly be substituted for Ca^{2+} in the medium before and during stimulation, thus allowing one to determine Me^{2+} fluxes. With our "model" cell, *Paramecium*, we showed that, upon stimulation (causing rapid Ca^{2+} mobilization from subplasmalemmal stores), Ca was immediately exchanged for Sr in stores.

Key Words: **calcium; cilia; EDX; electron microscopy; exocytosis; *Paramecium;* quenched-flow; secretion; X ray.**

INTRODUCTION

This paper takes into account two main aspects: (i) the importance of Ca^{2+} as a second messenger and (ii) the need to analyze total calcium concentrations, [Ca], and its dynamics, to understand the dynamics of free intracellular calcium, $[Ca^{2+}]_i$, in cells upon stimulation that finally triggers a variety of dynamic cellular processes.

Comparing free, ionic calcium concentrations at rest and after activation, respectively, normally in animal cells a $[Ca^{2+}]_i^{rest}$ of ~50 to 100 nM is registered, while amounts of $[Ca^{2+}]_i^{act}$ of ~500 nM to >10 (occasionally >100) μM may be required for full activation, depending on the system analyzed (Bootman and Berridge, 1995). Yet local $[Ca^{2+}]_i$ required to briefly activate "strategic" sites is much higher (Klingauf and Neher, 1997; Neher, 1998) and can be estimated only indirectly. Also $[Ca^{2+}]_i^{act}$ may originate from influx from the extracellular medium (Ca_e^{2+}), it may be liberated from stores by different activation mechanisms, or both mechanisms may cooperate in different ways (Berridge, 1998; Barritt, 1999; Mackrill, 1999). For instance, the mutual interactions between Ca^{2+} influx and Ca^{2+} mobilization from a subset of Ca stores closely associated with the cell membrane ("subplasmalemmal" or "cortical" calcium stores) are currently under considerable debate.

From the elaborate methods available to determine local $[Ca^{2+}]_i$ in cytosol or in some subcellular structures, like stores, different approaches must be combined to elucidate different aspects, such as temporal and spatial resolution (Nuccitelli, 1994; Klingauf and Neher, 1997; Verkhratsky and Toescu, 1998). Methods include not only imaging by Ca^{2+}-specific fluorochromes, but also laser activation of caged compounds and analysis of local $[Ca^{2+}]_i$ changes by injection of Ca^{2+} buffers with different affinity (K_d) or time constants. Clearly these approaches may cover most important functional aspects, although local values for total [Ca] and Ca^{2+} fluxes can be estimated only indirectly (Naraghi *et al.,* 1998).

[1] To whom correspondence should be addressed. Fax: 49-7531-88-2245. E-mail: helmut.plattner@uni-konstanz.de.

Values for [Ca] could easily be obtained, in principle, by analytical electron microscopic (EM) methods, such as energy-dispersive X-ray microanalysis (EDX) (Hall, 1979; Warley, 1997; Reimer, 1998). In this case, a main problem is Ca redistribution during preparation, although this can be overcome by cryofixation (fast freezing). This can operate on a millisecond-time scale and can avoid dislocation of Ca^{2+}, provided dislocation by ice crystal formation is minimized by high cooling rates down to low temperatures (Plattner and Bachmann, 1982; Sitte, 1996). Thus, cryofixation can theoretically combine high temporal (ms) resolution with high spatial (<100 nm) resolution for Ca localization in cells.

However, analytical EM analysis also faces important problems. Time-resolved analysis of fast processes requires coordination of cryofixation with stimulation of these processes. Our work is generally focused on synchronous exo–endocytosis and ciliary beat in *Paramecium* cells, whereby synchronization allows one to overcome this handicap (Plattner *et al.*, 1993). Spatial resolution in EM element analysis is another problem. For instance, (i) frozen-hydrated samples are difficult to analyze because of electrostatic charging, and (ii) freeze-dried samples, though frequently a recommendable alternative, may make identification of smaller details difficult, while (iii) freeze-substitution requires reliable retention of an individual element to be analyzed, e.g., by specific precipitation or chelation, while other elements are excluded from analysis. Although method (ii) may initially be considered superior, we show here that, with cell suspensions, method (iii) can fully match requirements for time-resolved [Ca] analyses by EDX in the subsecond time range.

Briefly, we subject our cells, the ciliated protozoan *Paramecium tetraurelia,* to stimulation by aminoethyldextran (AED, Plattner *et al.*, 1984, 1985, 1993) and cryofixation in the subsecond time range. Previously we had shown that the ~1000 dense-core-type secretory organelles ("trichocysts") docked at the cell membrane are amenable to immediate exocytosis within ~80 ms (all docked trichocysts in all cells during synchronous stimulation), followed by endocytosis of empty "ghosts" within ~350 ms (Knoll *et al.*, 1991; Plattner *et al.*, 1992; 1993). Analyses were carried out in a quenched-flow device previously described (Knoll *et al.*, 1991) and this could be combined with freeze-substitution in a medium containing OsO_4 and KF (forming insoluble CaF_2 or SrF_2, in Ca^{2+}/Sr^{2+} exchange experiments). In a *Paramecium* cell, cortical Ca stores ("alveolar sacs") can be easily pinpointed since they are tightly attached to the cell membrane in the form of flat sacs (Stelly *et al.*, 1991; Knoll *et al.*, 1993; Plattner *et al.*, 1997b). Alveolar sacs surround preformed exo–endocytosis sites and also closely approach the basis of each of the several thousand cilia (Plattner *et al.*, 1991). Cilia beat at ~20 Hz and the reversal of their beat activity is also regulated by Ca^{2+} (Machemer, 1988), though this normally comes from an influx through the ciliary membrane. AED primarily causes exocytosis in parallel with an increase of $[Ca^{2+}]$, from a basal level of ~60 nM at rest, to ~800 nM (according to fluorochrome analysis) or ~5 μM (according to Ca^{2+}-buffer injection) after activation (Klauke and Plattner, 1997). Any superposition of Ca^{2+} mobilization from stores by influx can be traced by Ca^{2+}/Sr^{2+} exchange during stimulation.

With or without such manipulations, cells can be triggered for different times with the polyamine, AED. AED stimulates not only synchronous exocytosis of all trichocysts (Plattner *et al.*, 1985, 1991; Knoll *et al.*, 1991), but frequently also entails ciliary (beat) reversal (Plattner *et al.*, 1985; Erxleben and Plattner, 1994). Previous work also had shown that Ca^{2+} is mobilized from alveolar sacs in the subsecond time range during AED stimulation (Knoll *et al.*, 1993; M. Hardt and H. Plattner, in preparation). Therefore, we considered this system appropriate for testing our approach to analyze Ca^{2+} dynamics by EDX (Fig. 1). Questions specifically addressed here serve mainly for illustrating the usefulness of our approach.

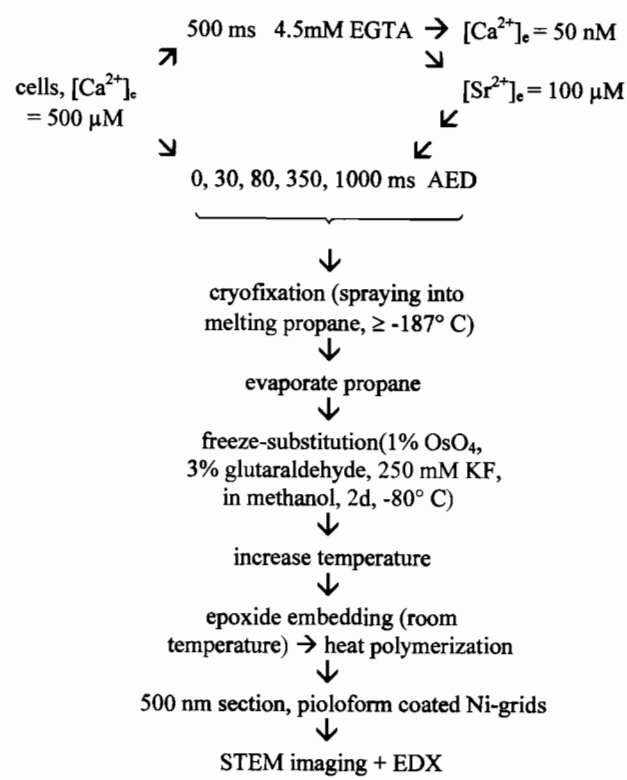

FIG. 1. Preparation flow chart, as explained in the text.

In our current approach, samples embedded in epoxy resin are analyzed by EDX, which determines total [Ca]. Local [Ca] is calibrated by different, mutually controlled standards. We calculate resolution of Ca localization in the sense of Ca detection limit (~2 mM) and structural correlation (~75 nm). This method now should allow determination of time-variable local [Ca], not only in closed compartments, but also in the cytosol. Our method can, thus, complement other methods available to estimate local [Ca] values, before and during activation and this paper serves to establish the validity of our method.

MATERIALS AND METHODS

Cells. *P. tetraurelia* cells, strain 7S, were cultivated axenically as described previously (Plattner *et al.*, 1997a). Cells were washed and kept for ~12 h in Pipes buffer (5 mM, pH 7), with $CaCl_2$ and KCl, 1 mM each, added.

Quenched-flow cryofixation and freeze-substitution. Cells were processed by quenched-flow as described previously (Knoll *et al.*, 1991). While we normally used $[Ca^{2+}]_e$ = 0.5 mM during AED stimulation, this method allows manipulation of $[Me^{2+}]_e$ as follows. Concentrations of Ca^{2+} and Sr^{2+} in the medium were eventually adjusted by mixing with 4.5 mM EGTA for 0.5 s, to final values calculated according to Bers *et al.* (1994) and indicated in the text. Calculations are based on values for EGTA of $K_d = 2.7 \times 10^{-7}$ M and 6.0×10^{-5} M for $[Ca^{2+}]$ and $[Sr^{2+}]$, respectively. While $[Ca^{2+}]_e$ was reduced to levels that would no longer support any of the functions analyzed, such as exocytosis and ciliary reversal, these reactions could be reestablished by adding an excess of Sr^{2+} during stimulation for 80 ms by AED (not shown).

Cells were further processed as described by Knoll *et al.* (1991, 1993), with variations indicated in Fig. 1. Essentially we pumped off the cryogen, propane, before cryofixed cells were freeze-substituted for 2 days at −80°C in the presence of 250 mM KF, 3% glutaraldehyde, and 1% OsO_4 in methanol. OsO_4 was used to avoid osmotic effects in subsequent steps (Plattner and Zingsheim, 1983), e.g., swelling of alveolar sacs. Then the temperature was increased at a rate of 5°C/h to room temperature. Finally cells were embedded in Spurr's epoxy resin and processed into 500-nm sections.

Standards for EDX analysis. We used two types of standards. (i) Organic Ca compounds at different concentrations in epoxide resin according to Chandler (1976; Dörge *et al.*, 1978) were obtained from British BioCell (Cardiff, Wales) or Plano (Wetzlar, Germany); (ii) Ca-exchange (Chelex) beads, according to DeBrujin (1981), incubated at different $[Ca^{2+}]$, were a gift from Bio-Rad

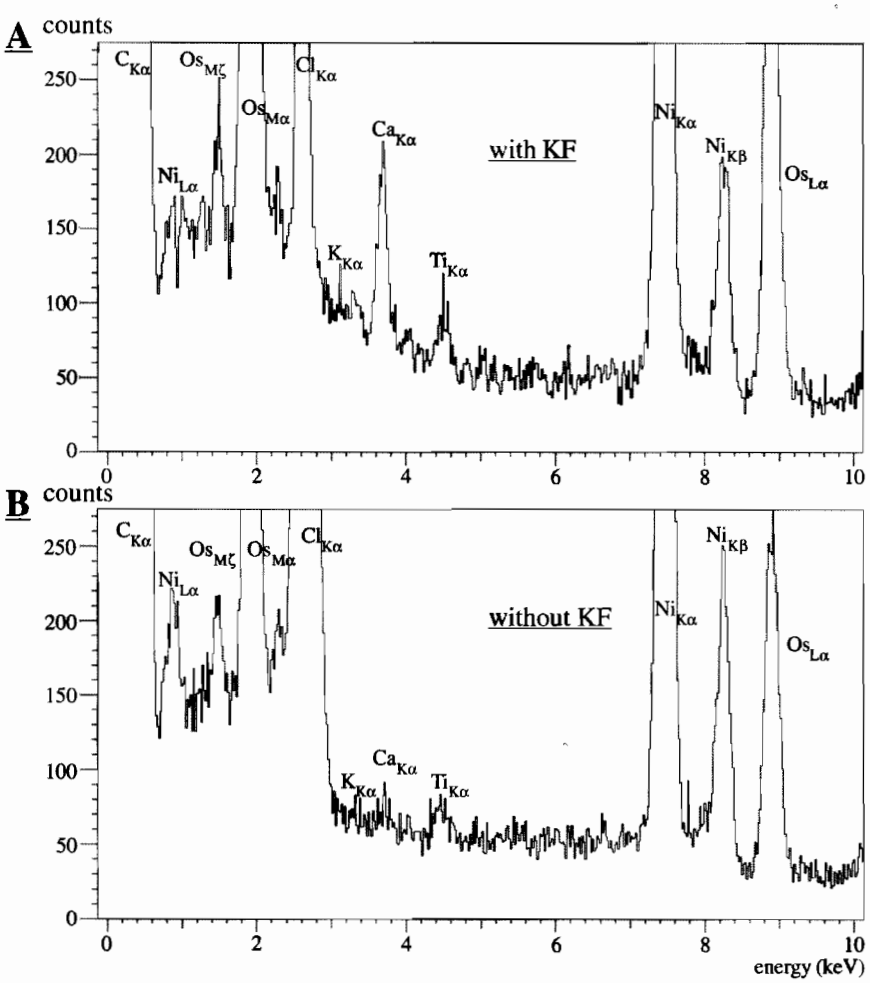

FIG. 2. Spectra obtained by spot measurements on alveolar sacs of an unstimulated cell, processed by quenched flow/fast freezing at $[Ca^{2+}]_e$ = 500 μM and freeze-substitution in the presence (A) or in the absence (B) of KF.

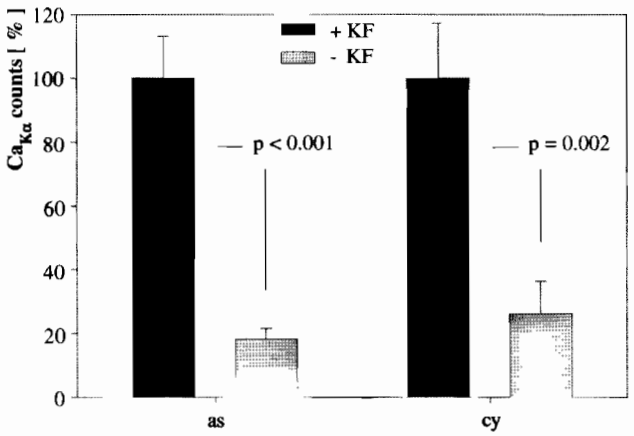

FIG. 3. Variability of CaK_α counts obtained by spot measurements on alveolar sacs or in the cytosol of an unstimulated cell (processed as indicated in the legend to Fig. 2), with KF present or absent during freeze-substitution, in two independent experiments (10 structures each collected from 10 cells). Normalized data (CaK_α signal = 100% for samples freeze-substituted in the presence of KF) reveal considerable signal loss from alveolar sacs (as) and cytoplasm (cy) when samples are processed without KF in the freeze-substitution medium. Bars denote SEM (standard error of the mean); *P* denotes significance level.

(Munich, Germany). After incubation, residual $[Ca^{2+}]$ in the medium was measured and Ca retained referred to dry mass of beads. [Ca] in standards was controlled by neutron activation in Actlabs Laboratories (Ancaster, Ontario, Canada) or by atomic absorption in the Perkin–Elmer Laboratories (Überlingen, Germany). Like cells, Chelex beads were embedded in Spurr's resin. From both types of standards we prepared sections for EDX analysis.

STEM and EDX analysis. Sections, usually 500 nm thick (as judged from previously calibrated interference colors), were mounted on Pioloform-coated nickel grids. Analysis was carried out in a Leo/Zeiss Model EM912Ω electron microscope operating in the STEM mode under the following conditions: 80-kV acceleration voltage, W-filament, ~10-μA emission current, 63-nm spot size (or 40 nm for line scans), $\sim 1.2 \times 10^9\ e^- \times \mu m^{-2} \times s^{-1}$ dose rate. Further conditions for EDX were as follows: ISO901 detection system from Oxford Instruments [(Wiesbaden, Germany), liquid N_2-cooled Li-drifted Si detector, front area 30 mm^2, sample–detector distance ~12.5 mm, ATW atmospheric window], 20° to 30° sample tilting, Link multichannel analyzer, Link Isis 3.00 software from Oxford Instruments, and in part software from Dr. L. Reimer (Münster/W., Germany). Counting rates were ≤2000 counts $\times\ s^{-1}$, keeping coincidences at ≤1%, effective sampling time of 100 s. From spectra recorded in spot measurements, specific signals in the range of 3.57 to 3.83 keV for CaK_α (3.691 keV) or 13.95 to 14.39 keV for SrK_α (14.143 keV) were evaluated by separating count integrals from the continuum, using a digital top-hat filter, for background correction, based on counts in the range of 5.11 to 5.38 keV or 15.01 to 15.45 keV, respectively. For this, Temquant software (Isis) from Oxford Instruments was used. For imaging and line scans we used Speedmap software, also from Isis. Eventually data were transformed into false color images.

RESULTS

Rationale of Methodical Approach and Resulting Preparation Schedule

Figure 1 outlines the preparative steps we performed. This may include manipulation of the extracellular medium. For instance, Ca_e^{2+} can be chelated by EGTA for 500 ms. This brief time period was selected in order to take into account the notorious sensitivity of our cells to low $[Ca^{2+}]_e$, while the reaction time of Ca–EGTA chelation to equilibrium is only ~0.20 ms (Neher, 1986; Adler *et al.*, 1991). This yields a calculated value of $[Ca^{2+}]_e = 50$ nM, i.e., below $[Ca^{2+}]_i^{rest} = 50$ to 70 nM (Klauke and Plattner, 1997). This step can be combined with adding an excess of Sr^{2+} to the trigger solution. Substitution of Ca_e^{2+} for Sr_e^{2+} is feasible, since Sr^{2+} drives normal exocytosis (M. Hardt and H. Plattner, in preparation) or ciliary beat activity (unpublished observations) in *Paramecium* cells.

Preparative Aspects of the Current Approach

Only with KF in the substitution medium could we retain Ca in alveolar sacs, as shown in the spectrum

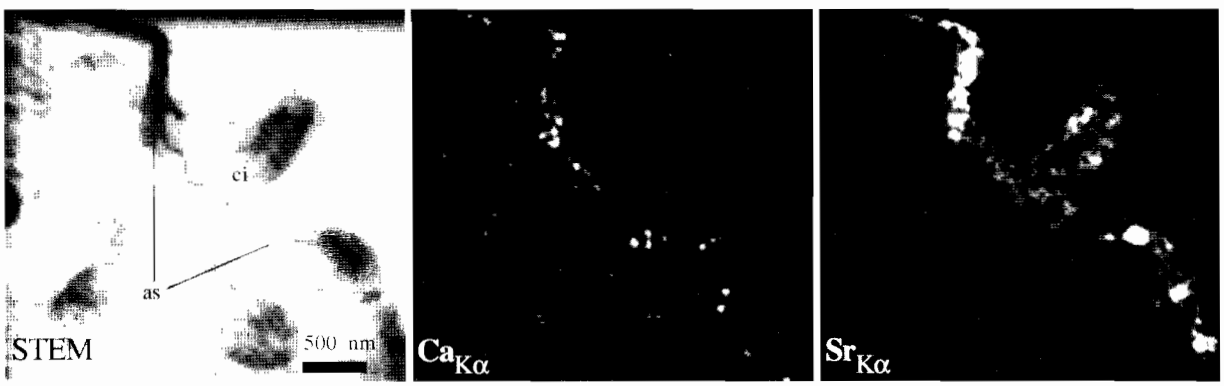

FIG. 4. Cortical structures and Me^{2+} localization in a *Paramecium* cell, processed as outlined in Fig. 1. (Left) STEM image showing a cilium (ci) and alveolar sacs (as). (Middle) CaK_α image. (Right) SrK_α image in false-color representation. The cell has been processed at $[Ca^{2+}]_e = 50$ nM (500 ms) followed by AED stimulation for 80 ms in presence of a calculated $[Sr^{2+}]_e = 100$ μM (with calculated residual $[Ca^{2+}]_e \sim 0.05$ μM). Note occurrence of abundant SrK_α signal in alveolar sacs and of some SrK_α signal in the cilium, while CaK_α signals are weak in alveolar sacs and not recognizable in the cilium.

of Fig. 2. Quantitative evaluation reveals that Ca did not leak into nearby cytosol, i.e., ~0.5 μm from stores (Fig. 3). Under any conditions used, the width of the alveolar sacs was constantly 100 nm (data not shown) and, thus, CaK_α signal measurements are directly comparable throughout our experiments.

The freeze-substitution approach with inclusion of KF, adapted from previous work by Poenie and Epel (1987) and Knoll *et al.* (1993), is applicable also to Sr. SrF_2, though approximately six times more soluble than CaF_2, also has a solubility of <1 mM, i.e., below the detection limit determined for EDX in our approach (see below). Specifically, solubility values available for 25°C are 0.231 and 0.955 mM, for CaF_2 and SrF_2, respectively (Goodenough and Stenger, 1973), and would be much lower at −80°C. Figure 4 gives an example of the Ca^{2+}/Sr^{2+} substitution in the medium during stimulation. The cell shown in Fig. 4 has been brought to $[Ca^{2+}]_e$ = 50 nM for 500 ms, while during the subsequent 80-ms AED stimulation a calculated value of $[Sr^{2+}]_e$ = 100 μM was provided. In element maps recorded under such conditions, CaK_α signals arising from alveolar sacs are considerably weaker than SrK_α signals, since Sr has replaced most of the Ca, as Ca^{2+} was released during stimulation and dissipated in the cytosol to levels below detectability.

How reproducible are CaK_α counts in Ca stores?

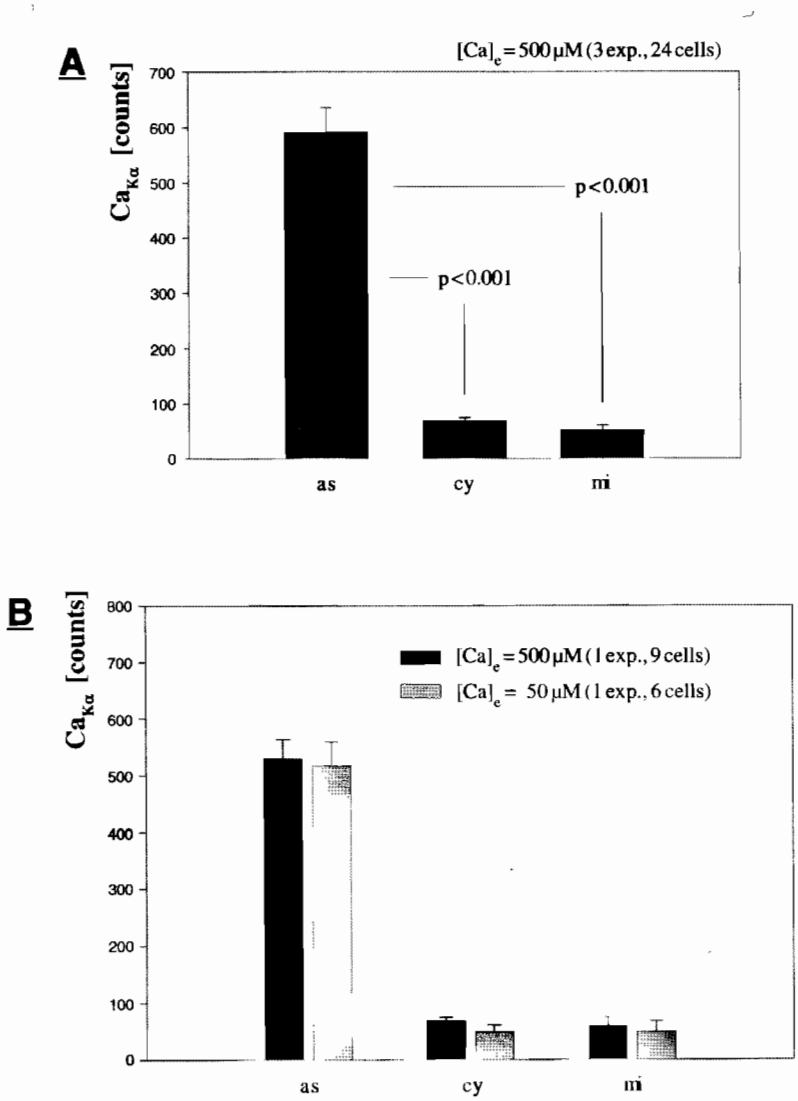

FIG. 5. Statistical analysis of calcium measurements. Unstimulated cells prepared as in Fig. 1. Structures analyzed are alveolar sacs (as), cytosol (cy), and mitochondria (mi). (A) Evaluation of a total of 24 cells pooled from three independent experiments, all at $[Ca^{2+}]_e$ = 500 μM. (B) Comparison of data from individual experiments conducted at $[Ca^{2+}]_e$ = 500 or 50 μM, respectively. Bars denote SEM. In (B) paired columns are not statistically significantly different. Note reproducibility of data in individual experiments, similarity of data independent of $[Ca^{2+}]_e$, selective enrichment of Ca in alveolar sacs (as), and rather low signal (background subtracted as indicated under Materials and Methods) in cytosol (cy) and mitochondria (mi).

For quantitation, spot measurements and net count evaluation of CaK_α signals (see Materials and Methods) are the method of choice. According to spectra in Fig. 2 and statistical evaluation in Fig. 3, KF is definitely required to retain Ca in alveolar sacs and cytosol. [Any effects of other X-ray fluorescence lines, like those of Os (in freeze-substitution medium) or Ni (from EM grid) seen in Fig. 2, will be addressed below]. [Ca] in the two compartments, with or without a membrane envelope, differs by a factor of ~10, but KF can well retain Ca locally in these widely different locations of a cell, with or without a membrane boundary.

Next we ascertained, again in unstimulated cells, the reproducibility of spot measurements (Fig. 5) in alveolar sacs, in the cortical cytosol (0.5 μm from a trichocyst docking site), and in mitochondria (contained in the cell cortex). In addition we checked any possible influence of varying $[Ca^{2+}]_e$. In Fig. 5A we evaluate data from three experiments, with a total of 24 cells at $[Ca^{2+}]_e$ = 500 μM. Data are quite reproducible, and alveolar sacs are the only cortical structures yielding relevant CaK_α signals. In Fig. 5B we compare individual experiments conducted at $[Ca^{2+}]_e$ of 500 or 50 μM. Data obtained with the two $[Ca^{2+}]_e$ values are quite similar, and data obtained in a single experiment are quite representative, as comparison of Figs. 5A and 5B shows.

Figure 6 shows that Ca is retained also in deep cell regions, like in the nuclear envelope, though its dimensions and Ca content are at the limits of detectability and require statistical data analysis.

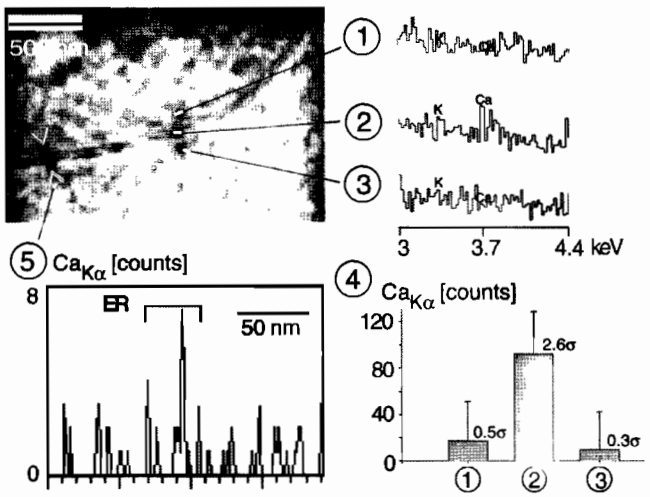

FIG. 6. Retention of Ca in the center of an unstimulated cell prepared as in Fig. 1, as exemplified for the ER (nuclear cisterna). In the STEM image, positions 1, 2, and 3 represent nucleoplasm, nuclear cisterna, and cytosol, respectively. In the corresponding spectra (right), there is an indication of a CaK_α signal only in the nuclear cisterna, which becomes more evident in the line scan (position 5) shown below, as well as in the statistical signal analysis at the bottom right [vertical lines = SD (standard deviation), σ = signal fluctuation [e.g., 2.6σ = 2.6 times SD)].

Analytical Aspects of Our Approach, Sensitivity, and Resolution

An example of STEM imaging and correlation with Ca or Sr imaging is presented in Fig. 4, which also displays the structures of interest, alveolar sacs and cilia.

For EDX, Pioloform-coated Ni grids enforced by evaporation of ~30-nm carbon were expected to yield more reproducible counting rates, yet the opposite was found. As Fig. 7 shows for alveolar sacs from samples mounted on carbon-coated grids, CK_α counts increase with time, most likely due to self-contamination, while CaK_α counts widely vary. Both, CK_α and CaK_α signals are much more constant and reproducible with non-carbon-coated grids, as they were used further on.

For standards with increasing [Ca], Ca^{2+} exchanger Chelex beads were incubated with increasing $[Ca^{2+}]$ according to DeBrujin (1981). Residual $[Ca^{2+}]$ in the solution was determined by atomic absorption and [Ca] retained in beads was controlled by neutron activation. Ca retained in beads was linear up to $[Ca^{2+}]$ = 200 mM (enriched from medium, as determined). Such beads were embedded in epoxy resin, just like cells, and 500-nm-thick sections were used for the following tests.

We recorded spectra by spot measurements at different locations of calibration beads and over different recording times (Figs. 8A, 8D, and 8E). [Ca] recorded in beads is homogenously distributed and CaK_α readings are constant with time. Then we performed line scans across the boundary of beads (Fig. 8B) to record STEM or CaK_α signals (Fig. 8C). CaK_α signals were further evaluated below, but already mere visual comparison of STEM and CaK_α signals in Fig. 8C clearly shows a strictly antiparallel increase/decay of theses two signals. Their inclination coefficient is quite similar, though the change of the X-ray signal on the bead boundary appears to be even more concise than that of the STEM signal (see below), thus indicating excellent CaK_α/structure correlation. Since this rather strict correlation of both signals also clearly excludes any significant Ca^{2+} leakage into surrounding embedding medium, we are confident about the reliability of recordings in cells, where most of the Ca is bound to proteins.

Figure 9 documents calibration with sections from two types of standards (designated types I and II): (i) epoxy resin with Ca^{2+} directly included at different concentrations (Chandler, 1976) and (ii) Ca^{2+}-impregnated Chelex beads as described above. *A priori*, Ca^{2+} loss cannot be a significant problem with type I standards, which, thus, can serve as addi-

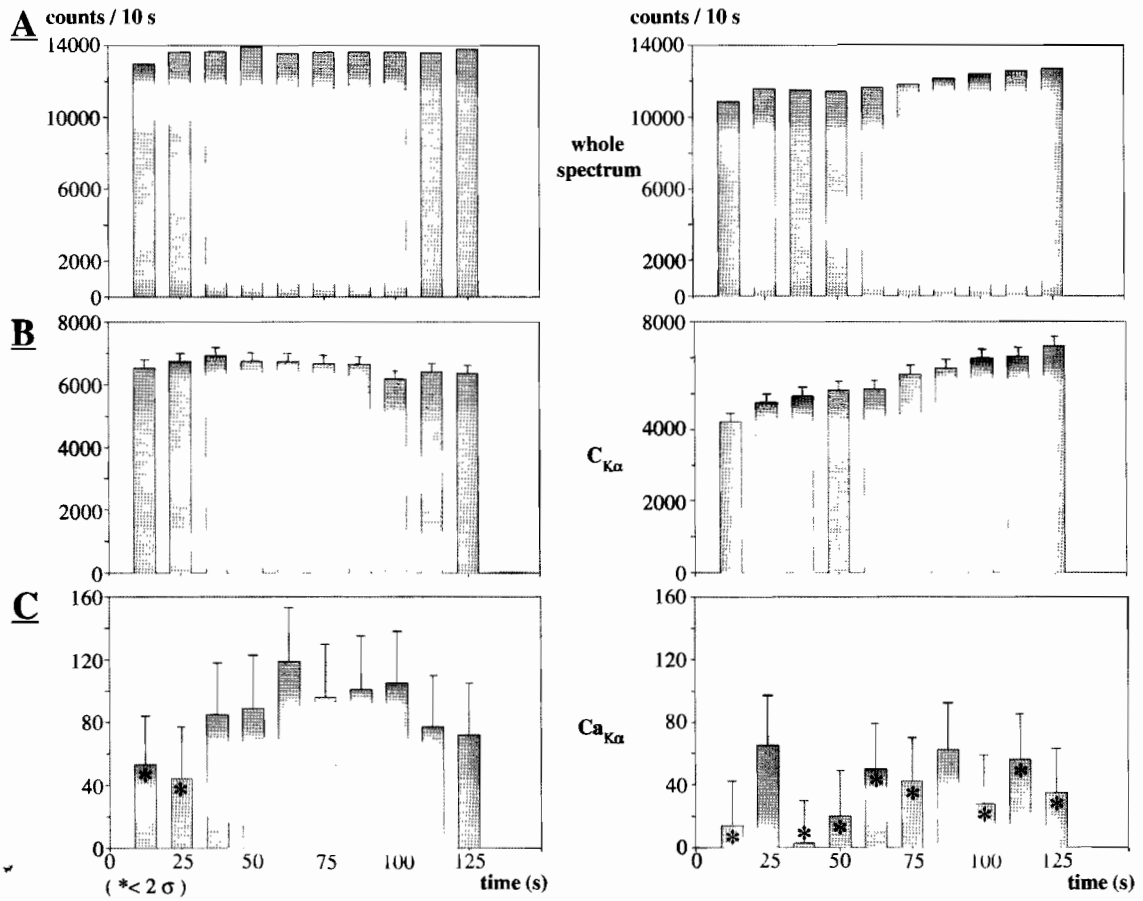

FIG. 7. Effect of absence (left) or presence (right) of carbon coating on Pioloform-coated nickel support grids on X-ray counts collected by spot measurements on alveolar sacs from unstimulated cells. Whole-spectrum counts are fairly similar and constant over analysis time (top). CK_α counts linearly increase during 125 s selectively on C-coated grids (middle), indicating self-contamination of the sample. CaK_α net counts are approximately two times higher and less fluctuating than in C-coated grids (as used throughout this paper), except for columns labeled with an asterisk, where CaK_α is not significantly above noise fluctuation. Bars denote SD; σ as in Fig. 6.

tional controls. Furthermore, we also recorded spectra from type I standards (Fig. 9A). Calculation of "residuals" for different X-ray energies (Reimer, 1998) shows high reliability for energies of >1.2 keV. In detail, element-specific counts in such a spectrum are separated from the background using a digital top-hat filter and calculated by fitting to respective default profiles using the Temquant software. The curve of the respective residuals is flat for energies ≥1.2 keV (Fig. 9B), indicating high reliability of the fitting and the calculation of the specific net counts for that range (e.g., for K_α signals of elements with atomic number, $Z > 11$). When standards of type I and II are compared (Fig. 9C), CaK_α net counts increase linearly with [Ca], with a cut-off at ~2 mM (= detection limit). CaK_α signals also increase linearly with mass, when CaK_α and CK_α signals are compared in sections of different thickness (Fig. 9D).

Another problem to be considered is fluorescence excitation and/or absorption effects by heavy metals, either Os from freeze-substitution medium or Ni from EM support grids (Fig. 10). As a grid bar is approached, CaK_α signals do not remarkably increase at low to moderate NiK_α counts, which level off at a distance of ≥2500 nm (Fig. 10A). Only with unusually high NiK_α counts would CaK_α counts increase (Fig. 10C). Nevertheless, 2.5 μm was selected as the minimal distance in our analyses. CaK_α readings increase slightly as OsL_α signals increase (Figs. 10B and 10D). We estimate a signal increase by 25% due to osmication of our cells (Fig. 10B). We corrected our biological data accordingly.

In Fig. 11 we summarize data on resolution and related parameters, particularly concerning correlation between CaK_α signal and structural detail in 500-nm sections. Beam broadening was calculated by software from L. Reimer (University of Münster/W., Germany). A primary electron beam of 63 nm enlarges only to 74 to 76 nm (90% cut-off), with or without Os in a sample, as calculated or as measured on contamination spots (Fig. 11B). The formula indicated in Fig. 11B for beam broadening is from the

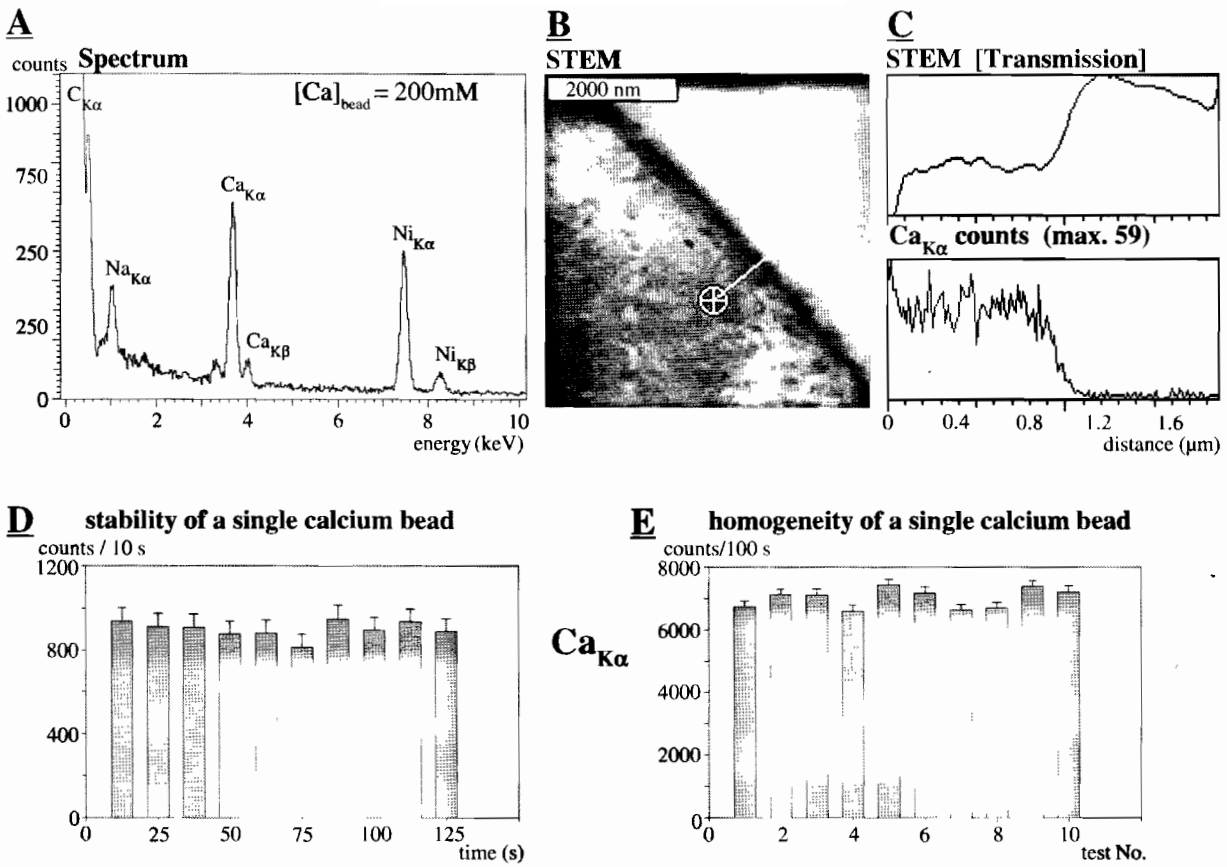

FIG. 8. Evaluation of Chelex Ca^{2+}-exchange beads ($[Ca^{2+}]$ = 200 mM in bead, 500-nm-thick section). (A) Spectrum. (B) In the STEM image of a median section, the line indicates the line scan evaluated for electron density (STEM) and CaK_α counts, respectively (C), starting at the asterisk; in lower part of (C), ordinate = 59 counts. (D) Stability of the CaK_α signal and (E) its homogeneity throughout a bead. Bars denote SD.

Isis program. Figure 11C (left) is derived from a line scan (spot diameter = 40 nm) through a Chelex bead boundary. Some other parameters related to resolution values were defined alternatively as mismatch of "edges" of STEM and EDX (CaK_α) signal (a_1), as 2.5 times the average amplitude fluctuation (a_2) or as half the value of the transition of the CaK_α signal to zero (a_3). This results in values of a_1 = 13.2 nm, a_2 = 29.1 nm, and a_3 = 30.8 nm, all with Os in samples (Fig. 11C), which impairs resolution only slightly. In sum, we conclude that we can achieve a structural correlation of CaK_α signals, i.e., a "useful" resolution of ~30 nm with the set-up used.

DISCUSSION

General Aspects

Considering the importance of Ca^{2+} signaling in such widely different cellular processes (Berridge *et al.*, 1998; Verkhratsky and Toescu, 1998), it is surprising that only a limited number of EDX analyses have been performed along these lines. These deal mostly with muscle contraction (Somlyo *et al.*, 1981; Wendt-Gallitelli and Isenberg, 1991) and with photoreceptor cell activation (Walz and Baumann, 1995). There are no analyses concerning ciliary beat regulation and none dealing directly with secretion regulation. As far as secretory systems have been analyzed, data reported aimed mainly at establishing concentrations of different ions particularly in secretory organelles, such as pancreatic zymogen granules (Roos and Barnard, 1985), and particularly the high [Ca] in a variety of secretory vesicles (Nicaise *et al.*, 1992). In previous EDX analyses of *Paramecium* cells, during AED stimulation, use of freeze-dried sections impeded any clear-cut correlation between CaK_α signals and alveolar sacs due to poor structural resolution, while it allowed, most importantly, one to establish the absence of any detectable [Ca] in trichocysts in the presence of high [Na] (Schmitz and Zierold, 1989).

Evaluation of Preparative Approach

As we show, the quenched-flow procedure used in conjunction with cryofixation and freeze-substitu-

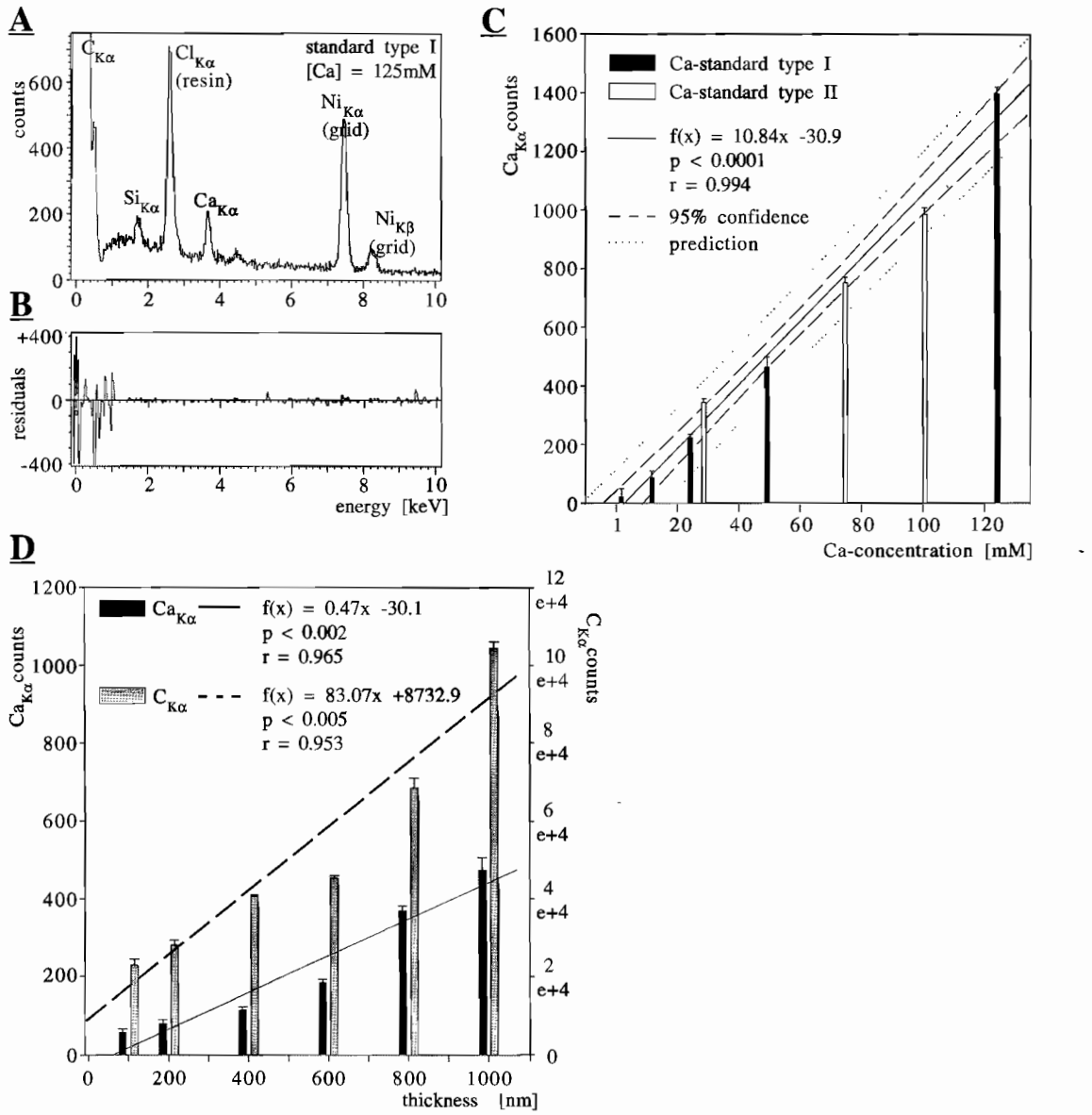

FIG. 9. Calibration of [Ca] measurements. (A) Spectrum recorded in type I standard (epoxy resin + Ca). (B) Residuals of the spectrum in (A) after calculation of the element-specific X rays by fitting to respective profiles. The flat part of the curve indicates a highly reliable calculation of element-specific X rays for energies of ≥1.2 keV. (C) [Ca]-dependent CaK_α counts obtained with 500-nm-thick sections from standards of type I (resin + Ca) and II (Chelex beads + Ca, in resin), respectively. The averaged regression line indicates a linear relationship between CaK_α recordings and [Ca] in samples, as well as a mean detection limit of ~2 mM. (D) Dependence of CK_α (indicative of mass thickness) and CaK_α signals on section thickness, showing a linear relation within the range of the section thickness used. Vertical lines on bars denote SD; r is the regression coefficient; "2 e + 4" to "12 e + 4" denotes 2×10^4 to 12×10^4 counts.

tion allows one to collect time-resolved data, in the subsecond time range, within well-defined structural entities. Retention of Ca (or Sr) is guaranteed by the low solubility of CaF_2 (or SrF_2) when KF is included in the freeze-substitution medium. Accordingly the signal almost disappears when KF is omitted. Addition of OsO_4 to the substitution medium abolishes osmotic swelling of organelles during subsequent processing. Hence, values obtained for local net CaK_α counts can easily be compared, e.g., in Ca stores since they maintain their well-defined width throughout our analyses (data not shown).

Our analyses show that Ca is retained not only in membrane-enveloped compartments, such as the Ca stores, but also in cilia and in the adjacent cytosol, when cells are stimulated by AED. Therefore, redistribution of Ca during processing is unlikely to occur and the redistribution observed can be clearly assigned to the stimulation effect. Another convincing argument is the clear-cut boundary of [Ca] in calibra-

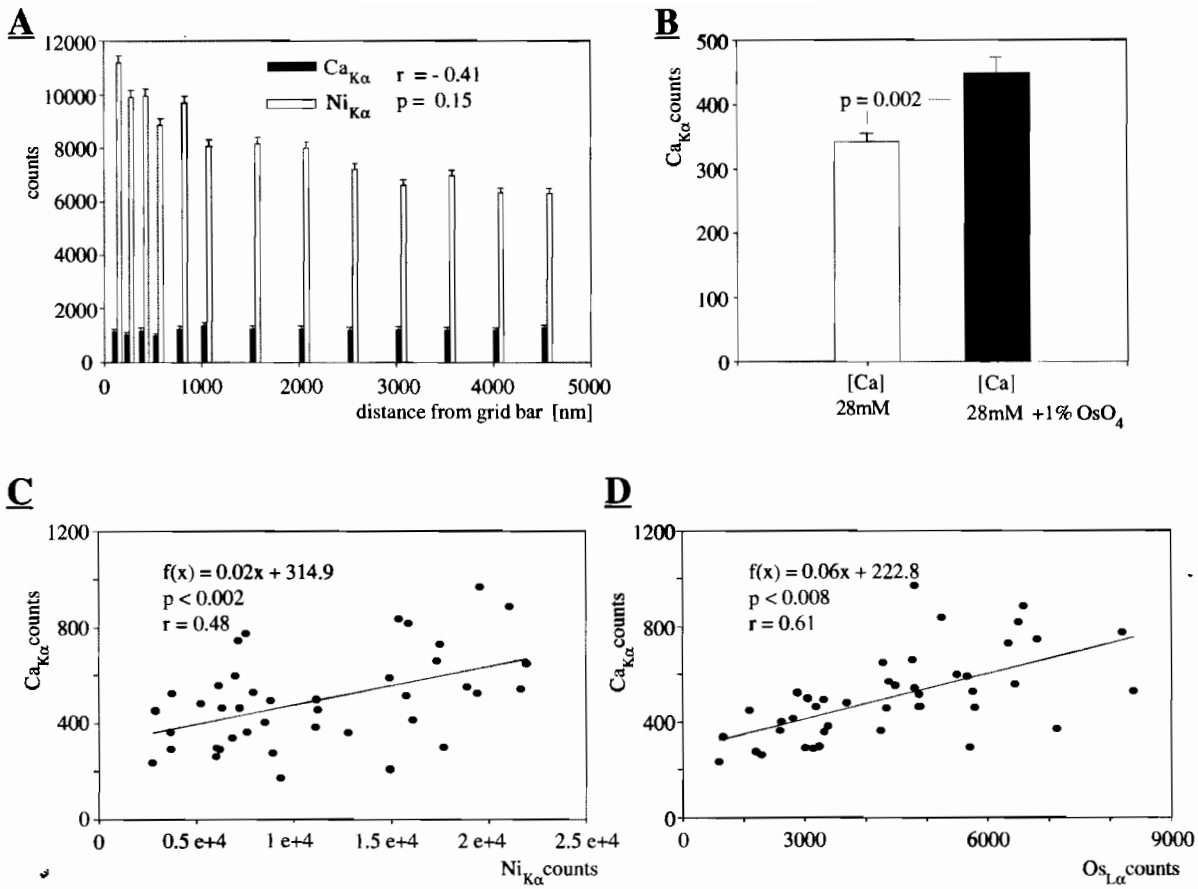

FIG. 10. Effects of Ni (from grid) and Os (from freeze-substitution) on CaK_α signals. Note that (with standard type I) CaK_α counts do not increase with NiK_α counts in (A), while NiK_α counts increase when a grid bar is approached to within ~2.5 μm, as is the case under such conditions with CaK_α signals recorded from individual alveolar sacs (C). Os-induced fluorescence (with standard type II, containing [Ca] = 28 mM) increases the CaK_α signal (B), statistically by ~25% (B) depending on actual OsL_α counts (D). The different effects of Ni and Os do not preclude the possibility that in a series of measurements on alveolar sacs, CaK_α counts may be positively correlated with both NiK_α counts (C) and OsL_α counts (D). "0.5 e + 4" to "2.5 e + 4" denotes 0.5×10^4 to 2.5×10^4 counts.

tion beads. Therefore, correlation of STEM signals and CaK_α signals in line scans through Chelex beads allowed us to establish values for resolution and to ascertain a useful EDX signal/structure correlation. As we show, the method presented is compatible with the size of structures actually analyzed.

Another important advantage of our method is the possibility of rapidly chelating Ca^{2+} in the medium and eventually of substituting Sr^{2+} for Ca^{2+} during stimulation, all in the subsecond time range. Both elements are functionally equivalent, as we have ascertained (unpublished observation) and their X-ray energies are quite resolvable in EDX. This allows one to trace intracellular Ca^{2+}/Sr^{2+} fluxes, e.g., when Ca^{2+} is released from alveolar sacs upon AED stimulation, while Sr^{2+} fills the stores by rapidly superimposed influx. These data are in line with the frequent observation that Sr^{2+} can drive different cell functions almost equally as well as Ca^{2+}.

Evaluation of Analytical Aspects

We have empirically optimized assay conditions with regard to CaK_α signal efficiency and EDX signal/structure correlation. This included optimization of section thickness, spot size, counting rates, etc., as outlined under Results. Under the analytical conditions finally selected, spot measurements combined with line scans and with statistical evaluation appear most useful. Analysis of EDX signals in spot measurements on strictly cross-cut or longitudinally cut organelles allows one to clearly assign EDX signals, e.g., to alveolar sacs, to ciliary bases, or to cilia. Eventually evaluation of element concentrations must take into consideration the size of any given structure in relation to section thickness. For instance, cilia in longitudinal section fill only half of a section and data must be corrected accordingly (while cross-cut cilia are larger than the excitation volume calculated, i.e., 250 nm vs 75 nm).

A **sensitivity** ≥ 2 mM (Ca)

energy resolution (FWHM)

5.9 keV $Mn_{K\alpha}$ ~ 133eV, 3.7 keV $Ca_{K\alpha}$ ~ 120eV, 3.3 keV $K_{K\alpha}$ ~ 120eV

structural resolution transmission signal (STEM)

experimental : ≤ 15 - 20 nm (linescans)

B

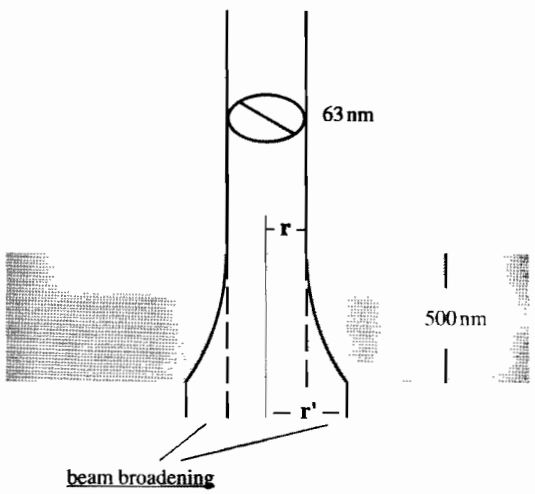

beam broadening
(spot size 63 nm)

type	with Os [nm]	without Os [nm]
calc.		
r'	37.2	36.9
meas.		
	N = 6	N = 5
r'	38.0 ± 4.5	37.5 ± 5.1

(mean ± std.dev. (σ))

$b\ (nm) = 625 \cdot 10^7 \cdot Z/E_0\ (\rho/A)^{1/2} \cdot (t \cdot 10^{-7})^{3/2}$

t = thickness, E_0 = incident beam energy, ρ = density, Z = atomic number, A = atomic weight

C

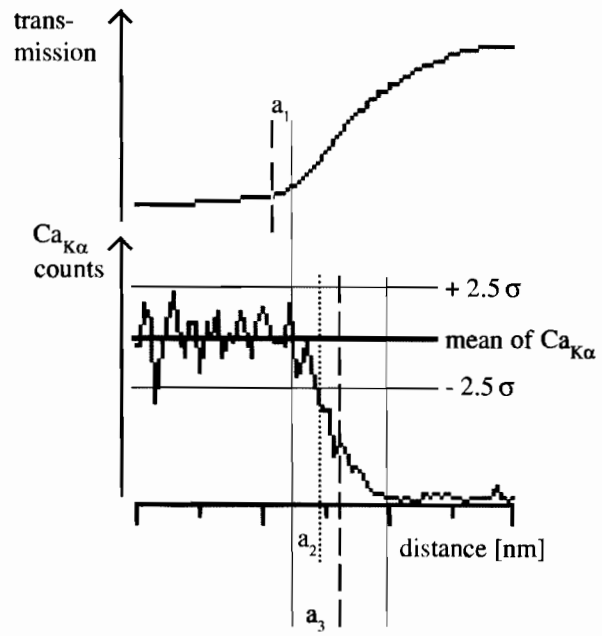

x-ray resolution
(linescans; spot size 40 nm)

type	with Os [nm], N=6	without Os [nm], N=5
a_1	13.2	11.0
a_2	29.1 ± 6.9	21.8 ± 5.9
a_3	30.8 ± 5.9	26.3 ± 4.2

(a_1 - median
$a_{2,3}$ - mean ± std.dev. (σ))

FIG. 11. Resolution achieved by the present EDX analysis (for details, see text). In (A) we summarize the detection limit ("sensitivity") derived from Fig. 7, X-ray energy resolution in relation to the standard MnK_α line, and resolution of the structural signal in STEM operation. FWHM, full width at half-maximum. (B) is a calculation of the broadening of a 63-nm beam due to diffusion of primary electrons in a 500-nm section, with or without osmication. (C) is a detailed analysis of the transmission signal and of the CaK_α X-ray signal, respectively, under operation conditions used, with or without osmication.

Negative methodical aspects to be avoided are carbon-coating of EM grids and fluorescence by nickel grids when too closely approaching grid bars. The fluorescence effect of Os, applied during freeze-substitution to provide sufficient electron contrast, requires correction of calculated [Ca] by ~25%, under our conditions. Beam broadening determined for a 500-nm section turned out to be almost negligible. Depending on definition, correlation of CaK_α X-ray signals with structural detail ("resolution") may be assumed as ~75 nm (primary electron beam diameter spread), i.e., slightly better than required to analyze alveolar sacs of ~95 nm in diameter.

For calibration we used different methods, with additional controls, as described. Only then were we confident about the high [Ca] = 43 mM in alveolar sacs. Simultaneously we noticed in the literature that most recent analyses tend to rather high [Ca] values, e.g., up to 50 mM estimated for sarcoplasmic reticulum (Meldolesi and Pozzan, 1998).

Conclusions

We use a quenched-flow procedure, operating in the subsecond time range, beyond a dead time of ≥30 ms, with time resolution ~1 ms (Knoll *et al.*, 1991). In the present paper we analyze preparative and analytical aspects pertinent to dynamic localization of Ca^{2+} by EDX analysis. Ca or Sr can be retained as insoluble fluorides during freeze-substitution (solubility <1 mM, i.e., below EDX detection limit), followed by epoxy resin embedding. Sections of 500 nm prove appropriate for STEM imaging and sufficiently resolved CaK_α signal, without any signs of any Me^{2+} leakage from stores in an unstimulated state, while stimulation entails significant Me^{2+} redistribution. EDX analysis is performed on a Zeiss/Leo EM912Ω electron microscope operated in the STEM mode. [Ca] is calibrated in different ways for mutual control, i.e., by epoxy resin-based Ca standards and by Ca^{2+} exchange beads (controlled by neutron activation and atomic absorption). The resulting concentration-dependent net signal increase is linear, between a cut-off at [Ca] = 2 mM (= detection limit) and a value of 200 mM (maximum tested). The [Ca] we find by EDX in the cytosolic compartment is close to current literature data values from other cells, as is our value for [Ca] in stores, i.e., ≤4 and 43 mM, respectively. Monte Carlo simulations (90% cut-off) yield a spread of primary electrons from a probe size of 63 to 75 nm, resulting in a spatial "resolution" of ~75 nm for X-ray signal/structure correlation. This is sufficient for analyzing Ca in the stores or in structures containing targets for Ca^{2+}. According to our EDX analysis, values for [Ca] (total) are 10^2 to 10^3 times the values for [Ca^{2+}] (free, ionic) recorded with fluorochromes. Thus, our method should be useful for total Ca^{2+} flux calculations.

For help, advice, and support, we thank Actlabs (Ancaster, Ontario, Canada), Dr. Bauer (Oxford Instruments, Wiesbaden, Germany), R. Bauer (Leo, Oberkochen, Germany), Bio-Rad (Munich, Germany), C. Braun (Konstanz, Germany), G. Brümmer (Leo, Oberkochen, Germany), Dr. J. A. Chandler (Cardiff, Wales, UK), Dr. W. C. DeBrujin (Rotterdam, The Netherlands), Dr. J. Hentschel (Konstanz, Germany), S. Kolassa (Konstanz, Germany), Dr. Erler (Perkin–Elmer Laboratories, Überlingen, Germany), and Dr. L. Reimer (Munich/W., Germany). This work was supported by the Deutsche Forschungsgemeinschaft Grant Pl 78/11 to H.P. within the Schwerpunkt "Neue mikroskopische Methoden für Biologie und Medizin."

REFERENCES

Adler, E. M., Augustine, G. J., Duffy, S. N., and Charlton, M. P. (1991) Alien intracellular calcium chelators attenuate neurotransmitter release at the squid giant synapse, *J. Neurosci.* **11,** 1496–1507.

Barritt, G. J. (1999) Receptor-activated Ca^{2+} inflow in animal cells: A variety of pathways tailored to meet different intracellular Ca^{2+} signalling requirements, *Biochem. J.* **337,** 153–169.

Berridge, M. J. (1997) Elementary and global aspects of calcium signalling, *J. Physiol.* **499,** 291–306.

Berridge, M. J. (1998) Neuronal calcium signaling, *Neuron* **21,** 13–26.

Berridge, M. J., Bootman, M. D., and Lipp, P. (1998) Calcium—A life and death signal, *Nature* **395,** 645–648.

Bers, D. M., Patton, C. W., and Nuccitelli, R. (1994) A practical guide to the preparation of Ca^{2+} buffers, *Methods Cell Biol.* **40,** 3–29.

Bootman, M. D., and Berridge, M. J. (1995) The elemental principles of calcium signaling, *Cell* **83,** 675–678.

Buchanan, R. A., Leapman, R. D., O'Connell, M. F., Reese, T. S., and Andrews, S. B. (1983) Quantitative scanning transmission electron microscopy of ultrathin cryosections: Subcellular organelles in rapidly frozen liver and cerebellar cortex, *J. Struct. Biol.* **110,** 244–255.

Chandler, J. A. (1976) A method for preparing absolute standards for quantitative calibration and measurement of section thickness with X-ray microanalysis of biological ultrathin specimens in EMMA, *J. Microsc.* **106,** 291–302.

DeBrujin, W. C. (1981) Ideal standards for quantitative X-ray microanalysis of biological specimens, *Scanning Electron Microsc.* **1981-II,** 357–367.

Dörge, A., Rick, R., Gehring, K., and Thurau, K. (1978) Preparation of freeze-dried cryosections for quantitative X-ray microanalysis in biological soft tissues, *Pflügers Arch. Eur. J. Physiol.* **373,** 85–97.

Erxleben, C., and Plattner, H. (1994) Ca^{2+} release from subplasmalemmal stores as a primary event during exocytosis in *Paramecium* cells, *J. Cell Biol.* **127,** 935–945.

Goodenough, R. D., and Stenger, V. A. (1973) Magnesium, calcium, strontium, barium and radium, *in* Bailar, J. C. (Ed.), Comprehensive Inorganic Chemistry, pp. 591–664, Pergamon, Oxford.

Hall, T. A. (1979) Biological X-ray microanalysis, *J. Microsc.* **117,** 145–163.

Klauke, N., and Plattner, H. (1997) Imaging of Ca^{2+} transients induced in *Paramecium* cells by a polyamine secretagogue, *J. Cell Sci.* **110,** 975–983.

Klingauf, J., and Neher, E. (1997) Modeling buffered Ca^{2+} diffusion near the membrane: Implications for secretion in neuroendocrine cells, *Biophys. J.* **72,** 674–690.

Knoll, G., Braun, C., and Plattner, H. (1991) Quenched flow analysis of exocytosis in *Paramecium* cells: Time course, changes in membrane structure, and calcium requirements revealed after rapid mixing and rapid freezing of intact cells, *J. Cell Biol.* **113,** 1295–1304.

Knoll, G., Grässle, A., Braun, C., Probst, W., Höhne-Zell, B., and Plattner, H. (1993) A calcium influx is neither strictly associated with nor necessary for exocytotic membrane fusion in *Paramecium* cells, *Cell Calcium* **14,** 173–184.

Länge, S., Klauke, N., and Plattner, H. (1995) Subplasmalemmal Ca^{2+} stores of probable relevance for exocytosis in *Paramecium.* Alveolar sacs share some but not all characteristics with sarcoplasmic reticulum, *Cell Calcium* **17,** 335–344.

Machemer, H. (1988) Electrophysiology, *in* Görtz, H. D. (Ed.), *Paramecium,* pp. 185–215, Springer-Verlag, Berlin/Heidelberg.

Mackrill, J. J. (1999) Protein–protein interactions in intracellular Ca^{2+}-release channel function, *Biochem. J.* **337,** 345–361.

Meldolesi, J., and Pozzan, T. (1998) The endoplasmic reticulum Ca^{2+} store: A view from the lumen, *Trends Biochem. Sci.* **23,** 10–14.

Naraghi, M., Müller, T. H., and Neher, E. (1998) Two-dimensional determination of the cellular Ca^{2+} binding in bovine chromaffin cells, *Biophys. J.* **75,** 1635–1647.

Neher, E. (1986) Concentration profiles of intracellular calcium in the presence of a diffusible chelator, *Exp. Brain Res.* **14,** 80–96.

Neher, E. (1998) Vesicle pools and Ca^{2+} microdomains: New tools for understanding their roles in neurotransmitter release, *Neuron* **20,** 389–399.

Nicaise, G., Maggio, K., Thirion, S., Horoyan, M., and Keicher, E. (1992) The calcium loading of secretory granules. A possible key event in stimulus–secretion coupling, *Biol. Cell* **75,** 89–99.

Nuccitelli, R. (1994) "A Practical Guide to the Study of Calcium in Living Cells," Academic Press, San Diego/New York/Boston.

Plattner, H., and Bachmann, L. (1982) Cryofixation: A tool in biological ultrastructural research, *Int. Rev. Cytol.* **79,** 237–304.

Plattner, H., Braun, C., and Hentschel, J. (1997a) Facilitation of membrane fusion during exocytosis and exocytosis-coupled endocytosis and acceleration of "ghost" detachment in *Paramecium* by extracellular calcium. A quenched-flow/freeze-fracture analysis, *J. Membr. Biol.* **158,** 197–208.

Plattner, H., Habermann, A., Kissmehl, R., Klauke, N., Majoul, I., and Söling, H. D. (1997b) Differential distribution of calcium stores in *Paramecium* cells. Occurrence of a subplasmalemmal store with a calsequestrin-like protein, *Eur. J. Cell Biol.* **71,** 297–306.

Plattner, H., Knoll, G., and Erxleben, C. (1992) The mechanics of biological membrane fusion. Merger of aspects from electron microscopy and patch-clamp analysis, *J. Cell Sci.* **103,** 613–618.

Plattner, H., Knoll, G., and Pape, R. (1993) Synchronization of different steps of the secretory cycle in *Paramecium tetraurelia:* Trichocyst exocytosis, exocytosis-coupled endocytosis, and intracellular transport, *in* Plattner, H. (Ed.), Membrane Traffic in Protozoa, Vol. 2A, pp. 123–148, JAI Press, Greenwich, CT/London.

Plattner, H., Lumpert, C. J., Knoll, G., Kissmehl, R., Höhne, B., Momayezi, M., and Glas-Albrecht, R. (1991) Stimulus-secretion coupling in *Paramecium* cells, *Eur. J. Cell Biol.* **55,** 3–16.

Plattner, H., Matt, H., Kersken, H., Haacke, B., and Stürzl, R. (1984) Synchronous exocytosis in *Paramecium* cells. I. A novel approach, *Exp. Cell Res.* **151,** 6–13.

Plattner, H., Stürzl, R., and Matt, H. (1985) Synchronous exocytosis in *Paramecium* cells. IV. Polyamino compounds as potent trigger agents for repeatable trigger-redocking cycles, *Eur. J. Cell Biol.* **36,** 32–37.

Plattner, H., and Zingsheim, H. P. (1983) Electron microscopic methods in cellular and molecular biology, *Subcell. Biochem.* **9,** 1–261.

Poenie, M., and Epel, D. (1987) Ultrastructural localization of intracellular calcium stores by a new cytochemical method, *J. Histochem. Cytochem.* **35,** 939–956.

Reimer, L. (1998) Scanning Electron Microscopy: Physics of Image Formation and Microanalysis, 2nd ed., Springer-Verlag, Berlin/Heidelberg/New York.

Roos, N., and Barnard, T. (1985) A comparison of subcellular element concentrations in frozen-dried, plastic-embedded, dry-cut sections and frozen-dried cryosections, *Ultramicroscopy* **17,** 335–344.

Schmitz, M., and Zierold, K. (1989) X-ray microanalysis of ion changes during fast processes of cells, as exemplified by trichocyst exocytosis of *Paramecium caudatum, in* Plattner, H. (Ed.), Electron Microscopy of Subcellular Dynamics, pp. 325–339, CRC Press, Boca Raton, FL.

Sitte, H. (1996) Advanced instrumentation and methodology related to cryoultramicrotomy: A review, *Scanning Microsc. Suppl.* **10,** 387–466.

Somlyo, A. V., Gonzales-Serratos, H., Shuman, H., McClellan, G., and Somlyo, A. P. (1981) Calcium release and ion changes in the sarcoplasmic reticulum of tetanized muscle: An electron-probe study, *J. Cell Biol.* **90,** 577–594.

Stelly, N., Mauger, J. P., Keryer, G., Claret, M., and Adoutte, A. (1991) Cortical alveoli of *Paramecium:* A vast submembraneous calcium storage compartment, *J. Cell Biol.* **113,** 103–112.

Verkhratsky, A., and Toescu, E. C. (1998) Integrative Aspects of Calcium Signalling, Plenum, New York/London.

Walz, B., and Baumann, O. (1995) Structure and cellular physiology of Ca^{2+} stores in invertebrate photoreceptors, *Cell Calcium* **18,** 342–351.

Warley, A. (1997) X-Ray Microanalysis for Biologists, Portland Press, London/Miami, FL.

Wendt-Gallitelli, M. F., and Isenberg, G. (1991) Total and free myoplasmic calcium during a contraction cycle: X-ray microanalysis in guinea-pig ventricular myocytes, *J. Physiol.* **435,** 349–372.